Laser Review

Dynamics of a Microparticle Levitated in Vacuum by an Optical Vortex Beam

Yoshihiko ARITA[1,2] and Kishan DHOLAKIA[1,3]

[1]*SUPA, School of Physics and Astronomy, University of St Andrews, St Andrews, Fife KY16 9SS, UK*

[2]*Molecular Chirality Research Center, Chiba University, 1-33 Yayoi-cho, Inage-ku, Chiba-shi 263-0022*

[3]*Graduate School of Engineering, Chiba University, 1-33 Yayoi-cho, Inage-ku, Chiba-shi 263-0022*

(Received January 31, 2018)

Levitated optomechanics is an emerging area of study enabled by optically trapped mesoscopic particles in vacuum. This opens the path to a range of new opportunities and insights at the classical-quantum interface. We review our recent work on the dynamics of an optically levitated microparticle in vacuum placed in an optical vortex beam. The dynamics are dictated by the orbital angular momentum of the field. The microparticle is confined within a Laguerre-Gaussian beam and orbits the annular beam profile with increasing angular velocity as the air drag force is reduced, as a result of reducing the background pressure. Furthermore, we extend this to explore the particle dynamics in a complex three-dimensional optical potential with orbital angular momentum in vacuum. The potential is formed by the generation of a "perfect vortex" beam, which upon propagation, evolves to a Bessel beam. We show that the optical gradient and scattering forces interplay with the inertial and gravitational forces acting on the trapped particle, which produces a rich variety of orbital motions with respect to the beam propagation axis.

Key Words: Laser trapping, Levitated optomechanics, Orbital angular momentum, Laguerre Gaussian beam, Perfect vortex beam

1. Introduction

The transfer of optical angular momentum to atoms, molecules, and mesoscopic particles offers new fundamental insights into the light-matter interaction as well as a variety of applications in optical manipulation. Spin angular momentum (SAM) is due to the polarization of light, whereas orbital angular momentum (OAM) is associated with an inclined wavefront, resulting in an azimuthal component to the Poynting vector of the light field. Such a field possesses a phase singularity, also called an optical vortex and can be described by a Laguerre-Gaussian (LG) mode. In the domain of optical manipulation, both types of angular momentum have been successfully transferred to microparticles in liquid and in air, leading to innovative studies including those of the fundamental aspects of the incident field, and applications of microrheology.[1-3]

Levitated optomechanics enables a range of new opportunities and insights at the classical-quantum limit.[4-10] Importantly, the absence of mechanical contact with the trapped object implies minimal dissipation. This leads to the realization of a high quality factor exceeding $Q > 10^{12}$ and has excellent potential for quantum metrological applications.[11,12] Whilst the majority of studies in this area have focused on linear momentum transfer, some recent studies have shown interest in angular momentum transfer to levitated microparticles,[13-16] including the transfer of OAM.[17,18] By including both SAM and OAM of light, a trapped particle can be a powerful testbed in levitated optomechanics to explore the particle's rotational degrees of freedom. The resulting complex orbital particle motion may have relevance to spin-orbit light-matter interactions[19,20] and quantum friction.[21]

In this article, we review our recent work on the transfer of OAM to dielectric silica microparticles in vacuum. We investigate particle motion around the annular profile of an LG beam, where the trapping beam's annular diameter is larger than the particle radius. We show that the trapping is two-dimensional (2D) and depends on interplay between the optical gradient and scattering forces, with contributions from inertial forces and gravity, which is in good agreement with theory.[17] We further extend this study to create a perfect vortex (PV) beam, which is the Fourier transform of a Bessel beam (BB). This means that over the three-dimensional (3D) space, the PV evolves on propagation to the BB, which has implications for the particle dynamics. The trapped microparticle in this instance exhibits a complex 3D orbital motion that includes a periodic radial motion between the PV and the BB.[22] This approach opens up new strategies for optical conveyors and transport in vacuum for atoms and mesoscopic particles.

2. Generation and characterization of LG beams

Our setup is based on a holographic optical trapping system.[17] A spatial light modulator (SLM, Hamamatsu LCOS-SLM X10468-03) is placed in a plane conjugate to the back aperture of the microscope objective (MO, Nikon E-Plan, × 100, NA = 1.25 in oil). This allows for the generation of LG modes with various topological charges and 3D positioning of the LG beam in the trap volume. We use the first diffraction order of a circularly apertured blazed grating to modulate the phase front of the incident light field. Any aberration is compensated for by the SLM with an unaberrated reference beam imaged at a plane conjugate to the sample.

An LG mode possesses an OAM of ℓ per photon, where ℓ is an integer that denotes the topological charge of the mode. For $\ell \neq 0$ and having a radial mode index $p = 0$, the phase singularity on the beam axis results in a zero axial intensity, which yields an annular beam profile. We first investigate the beam properties of the LG modes with linear polarization. Figure 1 shows the beam radius that scales linearly with the topological charge in the range of $4 \leq \ell \leq 11$. As the total power transmitted to the trap volume is maintained up to $\ell \leq 20$ (limited by the back aperture of the MO), the mean ring power density of the beam annulus decreases linearly with ℓ by assuming that the beam waist remains constant for different ℓ. The inset of Fig. 1 shows the annular beam profile of $\ell = 10$ where the intensity variation on the annulus is about 30% for two standard deviations (2σ).

3. Particle dynamics with an LG beam

In our experiment, we use a vacuum chamber with a volume of 27.7 $\mu\ell$, which has two optical glass windows (Harvard Apparatus, 8 mm in diameter, 150 μm in thickness) compatible with the MO used. Dry silica microspheres (Thermo Fisher Scientific, 5 μm in diameter) are preloaded onto one of the glass windows. A piezo electric transducer (APC International) affixed to the chamber is used to detach microspheres from the glass surface to load particles into the optical trap. Single silica spheres are trapped with linearly polarized light at a wavelength of 1070 nm with an optical power of 81.6 mW (measured at the back aperture of the MO). Once a single sphere is trapped in air, the chamber pressure is reduced to 10 kPa.

The optomechanics of a particle trapped with an LG beam is determined by a number of parameters: The optical torque transferred to the particle depends on the beam's topological charge ℓ, the mean ring power P of the LG beam, the annular radius of the orbit γ, as well as on the optical scattering properties of the silica particle. The Stokes drag coefficient Γ of the residual gas molecules plays an important role under vacuum, as the inertial force increases with rotation rate while the radial trapping force remains constant. This effect changes the particle trajectories in both the lateral and axial trapping positions. Figure 2(a) shows the trajectory of a silica sphere of 5 μm in diameter for the LG beam with $\ell = 10$ (indicated as dots), at a chamber pressure of 16.4 kPa, obtained from the center-of-mass (CoM) motion tracking using a fast framing CCD camera (3000 frames/s for 1 s).

The OAM transferred from the optical vortex drives the levitated silica microparticle once around the circumference with an orbital rate faster than 50 Hz. The dashed circle shows the annular beam profile of the LG beam with $\ell = 10$.

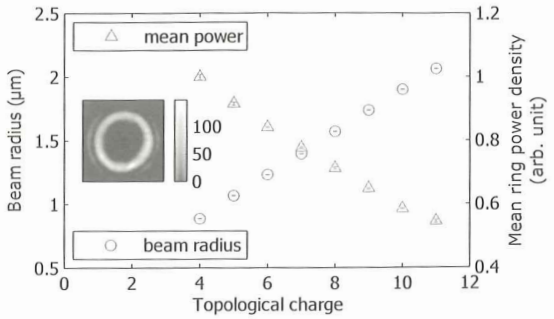

Fig. 1 Experimentally determined LG beam radius and mean ring power density dependent on the azimuthal index ℓ.[17] Error bars indicate 2σ.

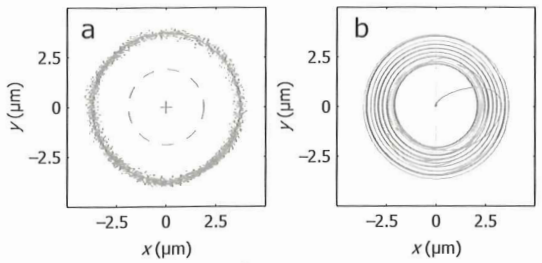

Fig. 2 Particle trajectories with different LG modes. (a) CoM positions (dots) of a particle trapped with $\ell = 10$, where the dashed circle indicates the annular beam profile. (b) Calculated orbital trajectories for $5 \leq \ell \leq 14$, where the orbital radius increases with ℓ.[17]

The discrepancy between the particle trajectory and the LG beam profile is due to the inertial force counteracting the radial trapping force both acting on the trapped particle.

Figure 2(b) shows the calculated orbital trajectories of a trapped particle for different topological charge ℓ. We use the numerical model based on a Mie scattering approach, where the optical force is determined directly from the optical eigenmodes of the system and calculated using the MATLAB EigenOptics package.[17] As the index ℓ increases, the orbital radius of the particle motion increases partly due to the scaling of the LG beams in size with ℓ [see Fig. 1]. More importantly the azimuthal force increases with ℓ, which leads to a faster orbital velocity of the particle. This in turn leads to an increase in inertial or centrifugal force and thus to an increase in the orbital radial position with respect to the radial trap [see Fig. 2(a)]. This outward force can be counteracted by the radial trapping force up to a maximal orbital velocity or rate with $\ell \leq 14$. When the inertial force exceeds the radial trapping force ($\ell \geq 15$), the particle leaves its azimuthal trajectory. On the other hand, for $\ell \leq 4$, no orbital motion is observed, as the diameter of the trapping beam (≤ 2.5 μm) is comparableor smaller than the particle radius. This leads to a stable particle trap in the center of the annular beam, thus canceling the orbital azimuthal forces. Figure 3 shows measured versus calculated orbital radius as a function of the azimuthal index ℓ. Our work shows that in the underdamped case there is a limit to the OAM transfer to a trapped, orbiting particle with LG beams.

4. Generation of perfect vortex beams

While an LG beam scales in size with azimuthal index ℓ

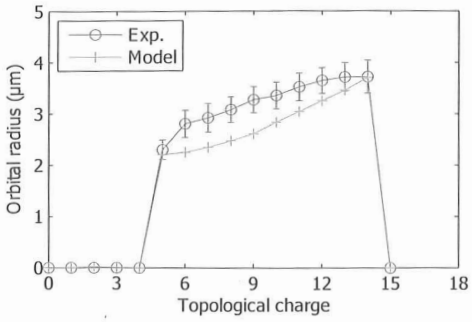

Fig. 3 Measured versus calculated orbital radius of the microparticle as a function of ℓ.[17] Error bars show 2σ.

[see Fig. 1], recently we have created a "perfect vortex" (PV) beam whose radial intensity profile is independent of ℓ , which has gained significant traction in optical manipulation in liquid media.[23,24] In order to create the PV, we use an axicon (apex angle of 178°) together with a suitable lens to generate an annulus in the far field. The annulus is projected on the SLM, whose plane is directly imaged onto the trapping plane with a series of lenses and the MO. The modulated first diffraction order is selected by a pinhole located at a Fourier plane and directed to the vacuum chamber for trapping a silica particle [Fig. 4].

When an axicon is illuminated with a Gaussian beam, a BB is formed in the near field, which transforms upon propagation to an annulus in the far field. In this way the BB is also formed at the conjugate plane of the pupil of the MO. Thus, a PV beam is the Fourier transform of a Bessel function and thus realizes an annulus with no spatial variation for differing ℓ values, in the trapping plane in contrast to a standard LG beams [see Fig. 1]. The topological charge of the beam is controlled by the vortex phase together with a grating phase applied on the SLM. The achievable topological charge is mainly limited by the back aperture of the MO due to the ring illumination used. In our system, we can create a PV beam with topological charges ranging from $-35 \le \ell \le 35$ without beam degradation. We note that, however, the beam profile is subject to aberrations arising from the refractive index mismatch between the optical system and the vacuum enclosure. So we restrict ourselves to topological charges $\ell \le |30|$.

5. Beam topography

Using a paraxial approximation of the beam propagation, one can simulate a PV starting from the axicon-generated annular beam at the SLM.[23] The beam profiles of such a PV along the propagation direction towards the BB are also well defined. Figures 5(a), (c), (e) show the simulated beam intensity profiles of a PV beam with $\ell = 15$, which is used for the particle levitation experiment. The axial view of the beam [Fig. 5(a)] is obtained as the sum of the beam profiles at different axial positions of $0 \le z \le 30$ µm [see Fig. 5(c)]. We note that the PV beam (50 µm in diameter) is formed at $z \approx 5$ µm in Fig. 5(c), which further propagates towards the concentric annular BB (10 µm in diameter) at $z \approx 30$ µm, where most of the beam power is available [Fig. 5(e)]. We note that the dimensions of the PV beam is determined by the lenses L_2 – L_4 and the MO, which project the annulus on the SLM to the TP, and is different from the corresponding LG beam [see Fig. 4].

We experimentally verify the beam propagation after a high-numerical-aperture MO, which is compared with the theoretical model [see Fig. 5(b), (d), (f)]. These experimental beam profiles are in good agreement with the simulation, both yielding a cone-shaped annular beam profile.

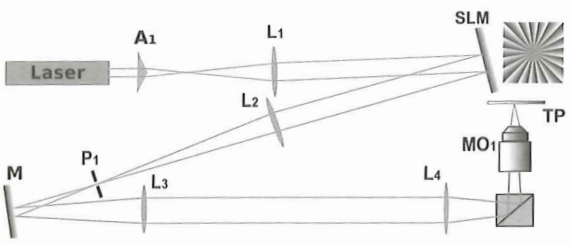

Fig. 4 Schematic of the experimental setup to create aperfect vortex beam (cw, 1070 nm) for trapping,[23] whereA_1 is an axicon, L_1-L_5 are a series of lenses, MO_1 is a microscope objective and TP denotes a trapping plane.

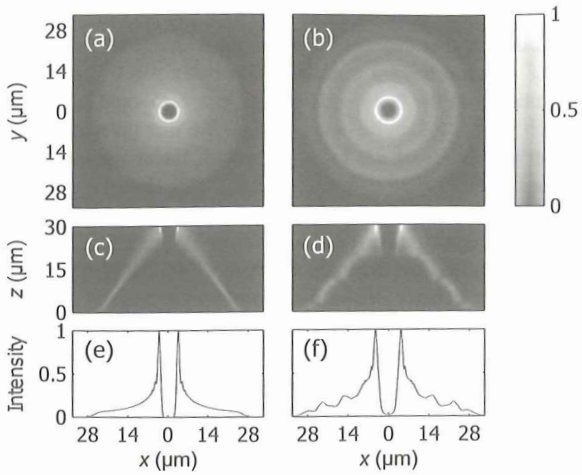

Fig. 5 Spatial profile of a perfect vortex beam with $\ell = 15$ propagating along the z-axis. Numerical simulations in (a), (c), (e) are compared with experimental beam profiles in (b), (d), (f).[22]

6. Particle dynamics in a perfect vortex beam

Figure 6 shows the trajectories of a silica particle (5 µm in diameter) trapped with a PV beam of $\ell = 15$ with an optical power of 81.6 mW at a chamber pressureof 5.5 kPa. The crossed markers represent the CoM positions of the particle recorded at every 2.1 ms. The inset shows the path of the particle through one complete cycle.

In order to understand its complex orbital motion, we show a 3D topography of the PV beam with $\ell = 15$ [see Fig. 7], where the grayscale gradient indicates the relative intensity of the beam. Here we include a schematic of the particle motion that depicts its trajectory: (i) trapped and set into rotation at the BB; (ii) horizontally launched into free space and lands on the PV beam; (iii) driven by both the scattering and gradient

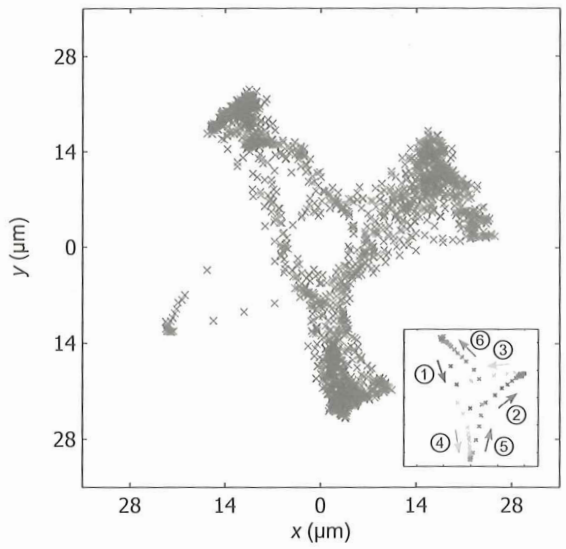

Fig. 6 Particle trajectories around the perfect vortex and Bessel beams with $\ell = 15$.[22]

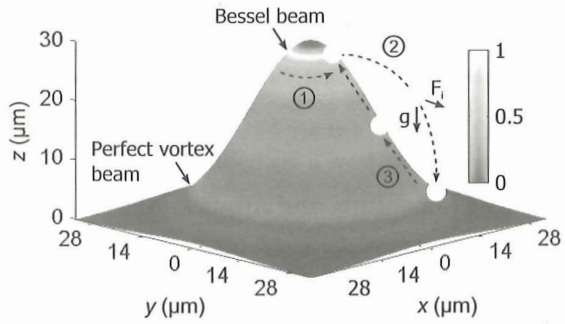

Fig. 7 Topography of the measured perfect vortex and Bessel beams around the beam axis ($x = y = 0$ μm) with a schematic of particle motion.[22]

forces towards the BB, where the particle restarts its orbital cycle, but its radial excursion can be branched into different directions [see Fig. 6]. We note that microparticles trapped with different topological charges undergo different trajectories. The radial rangethat microparticles explore depends on ℓ, which determines the orbital velocity at the annular BB, which in turn changes the outward inertial force.[22]

7. Characterization of a complex optical potential

As a particle can be stably trapped and continue its orbital motion typically for a duration of several hours, it is possible to quantify the particle velocity and the corresponding Stokes drag force F_S at any radial position relative to the PV beam using time-resolved images of the trapped particle. Once the local force field is probed by the single microparticle moving around the optical potential, one can establish a 1D map of the Stokes drag force F_S depending on the radial position r of the beam. The optical potential for the microparticle can be determined by the radial dependence of $F_S(r')$ as $U(r') = -\int F_s(r')dr'$.

Figure 8 shows the optical potential (solid line)determined by the particle moving around the trapping beam. For dielectric particles, the optical potential of the gradient force linearly scales with the optical field intensity as $U(r) = \alpha|E(r)|^2/2$, where α is the particle polarizability. The potential curve (solid line) is further fitted with the beam intensity profile [see Fig. 5(f)] averaged over the particle diameter of 5 μm (dashed line) using a nonlinear least squares fitting method available in MATLAB. Here we find a good agreement between the

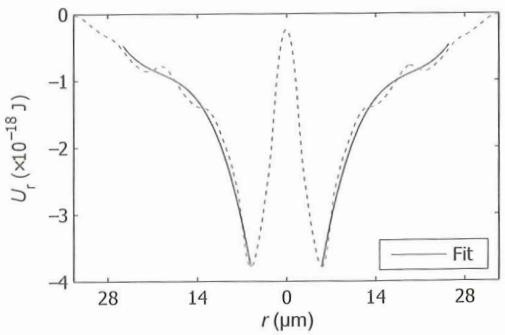

Fig. 8 Experimentally determined optical potential(solid line) probed by a microparticle moving around the beam axis ($r = 0$ μm). This potential curve is further fitted with the beam intensity profile averaged over the particle diameter of 5 μm (dashed line).[22]

two curves with a residual error < 5%. As such, the optical potential is characterized by the microparticle moving around the complex potential and yielded the deepest potential well of -3.8×10^{-18} J (~900 k_BT, where k_B is the Boltzmann constant and T is the temperature) at the annular BB.

8. Conclusions

In conclusion, we have reviewed our recent work on mesoscopic particle rotation in vacuum within a light field possessing OAM both in LG and PV beams. In the underdamped case, the particle inertia plays an important role in its dynamics, where the optical gradient and scattering forces interplay with the inertial and gravitational forces acting on the trapped particle. Our work shows that there is a limit to the possible OAM transfer to a trapped, orbiting particle. In the case of PV, the trapped microparticle exhibits a complex 3D orbital motion that includes a periodic radial motion between the PV and the BB. As the particle explores the whole 3D volume not solely restricted to one anchor point, it is possible to determine the 3D optical potential in situ by tracking the particle. This approach can open up the possibilities for a new geometry of cavity optomechanics, where a single particle orbits in and out of the optical cavity.

References

1) M. E. J. Friese, T. A. Nieminen, N. R. Heckenberg, and H. Rubinsztein-Dunlop: Nature **395** (1998) 621.
2) V. Garces-Chavez, D. McGloin, M. J. Padgett, W. Dultz, H. Schmitzer, and K. Dholakia: Phys. Rev. Lett. **91** (2003) 093602.
3) J. E. Curtis and D. G. Grier: Phys. Rev. Lett. **90** (2003) 133901.
4) A. Ashkin and J. M. Dziedzic: Appl. Phys. Lett. **19**(1971) 283.
5) T. Li, S. Kheifets, D. Medellin, and M. G. Raizen: Science **328** (2010) 1673.
6) T. Li, S. Kheifets, and M. G. Raizen: Nat. Phys. **7** (2011) 527.
7) P. F. Barker: Phys. Rev. Lett. **105** (2010) 073002.
8) D. E. Chang, C. A. Regal, S. B. Papp, D. J. Wilson, J. Ye, O. Painter, H. J. Kimble, and P. Zoller: *Proc. Natl. Acad. Sci. USA* **107** (2010) 1005.
9) J. Gieseler, B. Deutsch, R. Quidant, and L. Novotny: Phys. Rev. Lett. **109** (2012) 103603.
10) L. P. Neukirch, E. von Haartman, J. M. Rosenholm, and A. N. Vamivakas: Nat. Photonics **9** (2015) 653.
11) J. Gieseler, L. Novotny, and R. Quidant: Nat. Phys. **9** (2013) 806.
12) A. A. Geraci, S. B. Papp, and J. Kitching: Phys. Rev. Lett. **105** (2010) 101101.
13) Y. Arita, A. W. McKinley, M. Mazilu, H. Rubinsztein-Dunlop, and K. Dholakia: Anal. Chem. **83** (2011) 8855.
14) Y. Arita, M. Mazilu, and K. Dholakia: Nat. Commun. **4** (2013) 2374.
15) Y. Arita, M. Mazilu, T. Vettenburg, E. M. Wright, and K. Dholakia: Opt. Lett. **40** (2015) 4751.
16) S. Kuhn, P. Asenbaum, A. Kosloff, M. Sclafani, B. A. Stickler, S. Nimmrichter, K. Hornberger, O. Cheshnovsky, F. Patolsky, and M. Arndt, Nano Lett. **15** (2015) 5604.
17) M. Mazilu, Y. Arita, T. Vettenburg, J. M. Auñón, E. M. Wright, and K. Dholakia: Phys. Rev. A **94** (2016) 053821.
18) L.-M. Zhou, K.-W. Xiao, J. Chen, and N. Zhao: Laser Photon. Rev. **11** (2017) 1600284.
19) K. Y. Bliokh and Y. P. Bliokh: Phys. Rev. Lett. **96** (2006) 073903.
20) O. Hosten and P. Kwiat: Science **319** (2008) 787.
21) R. Zhao, A. Manjavacas, F. J. G. de Abajo, and J. B. Pendry: Phys. Rev. Lett. **109** (2012) 123604.
22) Y. Arita, M. Chen, E. M. Wright, and K. Dholakia: J. Opt. Soc. Am. B **34** (2017) C14.
23) M. Chen, M. Mazilu, Y. Arita, E. M. Wright, and K. Dholakia: Opt. Lett. **38** (2013) 4919.
24) M. Chen, M. Mazilu, Y. Arita, E. M. Wright, and K. Dholakia: Opt. Rev. **22** (2015) 162.